frontiers in Nanotechnology

ORIGINAL RESEARCH
published: 12 May 2021
doi: 10.3389/fnano.2021.667453

Moderately Transparent Chitosan-PVA Blended Membrane for Strong Mechanical Stiffness and as a Robust Bio-Material Energy Harvester Through Contact-Separation Mode TENG

Ravi Kumar Cheedarala and Jung Il Song**

Department of Mechanical Engineering, Research Institute of Mechatronics, Changwon National University, Changwon-Si, South Korea

OPEN ACCESS

Edited by:
Sima Umrao,
Indian Institute of Science, India

Reviewed by:
Tejendra Kumar Gupta,
Amity University, India
Sumanta Kumar Karan,
Pennsylvania State University, United States

***Correspondence:**
Ravi Kumar Cheedarala
rkchidrala@gmail.com
Jung Il Song
jisong@changwon.ac.kr

Specialty section:
This article was submitted to Nanotechnology for Energy Applications, a section of the journal Frontiers in Nanotechnology

Received: *13 February 2021*
Accepted: *06 April 2021*
Published: *12 May 2021*

Citation:
Cheedarala RK and Song JI (2021) Moderately Transparent Chitosan-PVA Blended Membrane for Strong Mechanical Stiffness and as a Robust Bio-Material Energy Harvester Through Contact-Separation Mode TENG. Front. Nanotechnol. 3:667453. doi: 10.3389/fnano.2021.667453

The detection of sustainable materials from naturally available resources using a simple fabrication process is highly important for novel research. Here, we used chitosan-PVA (Chs-PVA) blend films via layer-by-layer casting technologies for generating power through mechanical induction through triboelectric nanogenerators. The proposed Chs-PVA biodegradable film (i.e., thickness of 60 ± 5 μm) is facile, ecofriendly, highly flexible, mechanically strong, cost-effective, and easy to scale up. FT-IR analysis of the ChS-PVA blend membrane showed the strong interactions between the amines of ChS and hydroxyl groups of PVA through chemical cross-linking by hydrogen bonding. More importantly, the triboelectric nanogenerators (TENG) values of ChS-PVA films were 3–4 orders of magnitude lower than chitosan films reported before. Layer-on-layer cast films in particular exhibited high tensile strength (15.8 ± 1 MPa) and were more than three times stronger than other polyelectrolyte multilayer films. Both types of films remained stable in an acidic environment. Furthermore, the layer-on-layer-assembled films presented greater open circuit voltage (Voc) and short circuit current (Isc) values compared to pure ChS and PVA films. The ChS-PVA membrane can be used as a functional layer to produce charges by collecting get-up-and-go through vertical contact and separation mode TENG counters to the PVDF membrane. The enhancement of Voc and Isc of ChS-PVA TENG were 244 and 1,080% from ChS TENG. Where in the case of PVA TENG, the enhancement of Voc and Isc were increased by 633 and 2,888%, respectively due to the availability of free loan pair on the -NH_2 and -OH functional groups. The novel ChS-PVA TENG is a potential candidate for satisfying the tight requirement of an optimized energy harvesting device as an alternate bio-material option for contact-separation mode TENGs.

Keywords: chitosan, polyvinyl alcohol, chitosan-polyvinyl alcohol, triboelectric nanogenerators, open-circuit voltage, Short-circuit current

INTRODUCTION

Energy hunting through sustainable pathways has emerged with broad interests and pervasive impacts for addressing global energy issues and enabling feasible choices for working electronics and sensors in developing technologies for the application of wearable and implantable devices (Jiao et al., 2015; Zhu et al., 2015; Lin et al., 2016; Chen and Wang, 2017; Zhang et al., 2017). Triboelectric nanogenerators (TENGs) are capable of efficiently harvesting ubiquitous mechanical energy through contact triboelectrification and the electrostatic induction process (Fan et al., 2012; Yang et al., 2013; Zhang et al., 2013; Xie et al., 2014; Jiang et al., 2016; Maiti et al., 2019; Karan et al., 2020). With the growing intimidation of energy disaster and environmental degradation by global warming, scientists are seeking alternative routes for harvesting energy that can substitute conservative sources, for example solar, wind, and tidal energies, etc., (Maiti et al., 2019; Karan et al., 2020). Numerous categories of energy harvesting systems were industrialized to collect energy from the environment such as piezoelectric, thermoelectric, photoelectric, electrostatic, and electromagnetic procedures (Xie et al., 2014; Lin et al., 2016). Yet, environment-friendly, cost-effective, and reproducible energy collecting structures are strongly needed to satisfy the trade demand. Machine-driven energy is a natural renewable energy source that could be captured from human motion, etc. (Karan et al., 2020). In recent times, triboelectric nanogenerators (TENGs) have received worldwide consideration for the harvesting of sustainable energy from ambient resources. TENGs were established based on the amalgamation of contact and separation electrification to scavenge attenuated mechanical energy using materials which are in the triboelectric series (Fan et al., 2012; Yang et al., 2013). A suitable choice of triboelectric-paired tools and their rational strategy are able to increase the rate of harvesting energy and transformation efficiency (Zhang et al., 2013; Jiang et al., 2016). In consistent intermissions of contact with oppositely charged surfaces, electrons are motivated to movement through the exterior load and produce a continuous current (Wang et al., 2015). However, TENGs made of naturally plentiful biological resources have received limited attention (Zhang et al., 2013; Wang et al., 2015; Zhang et al., 2016). The consumption of natural waste materials for harvesting missed power-driven energy is of attention not only for important scientific investigation but also for addressing practical collective needs. Until now, chitosan-based natural polymer films have not been studied except for one article reporting the development of TENGs. Wang et al. studied laser-treated chitosan biopolymers for workable and biodegradable mechanical power creation through modified chitosan films and they obtained open circuit voltages and short circuit currents up to 2 V and <20 nA, respectively (Wang, 2013; Moon et al., 2017). However, to enhance the Voc and Isc of the chitosan membrane, we modified natural chitosan and Polyvinyl alcohol blend films. Here, we were motivated to utilize an amalgamation of a modified chitosan (Chs) and polyvinyl alcohol (PVA) blend membrane-based TENG (ChS-PVA-TENG) as an effective charge transmission source with a counter electronegative PVDF membrane (Chen et al., 2013; Tang et al., 2014; Shin et al., 2016) aimed at the contact separation electrification process. Recently, Wu et al. introduced chitosan-based laser-processed biopolymers for sustainable and biodegradable TENGs to generate power for the first time (Feng et al., 2018).

Chitosan (ChS) is one of the abundant biopolymers found in nature with great significant applications due to many active functional groups such as –OH and $–NH_2$ with constant natural nano to micro sized pores. Current utilization of ChS comprises various applications such as water treatment (Wang et al., 2017; Feng et al., 2018; Wang et al., 2018), drug delivery (Chen et al., 2013), maquillages (Mallineni et al., 2017), and skin care (Tang et al., 2014). These wide applications are due to the seasonal variations in configurations and degrees of polymerization of basic units which gives rise to the various physical and chemical properties (Chen et al., 2013; Shin et al., 2016). An ecological way to utilize this cheap and plentiful resource is highly anticipated (Yang et al., 2014c). ChS is obviously degradable, biocompatible, and has low cytotoxicity; ChS displays great potential as functional ingredients in biomedical strategies (Yang et al., 2013). Here, we chose to develop an economically viable, recyclable, and bendable triboelectric nanogenerator based on chitosan (ChS) and other natural materials such as Polyvinyl alcohol (PVA). By adjusting the PVA concentrations, the ChS-PVA nanocomposites are shown to have enhanced triboelectric power generation, altering the natural waste materials into robust functional energy devices with tunable mechanical and material properties. The ChS-PVA TENGs presenting well-organized energy conversion may cover the method concerning the economically feasible and environmentally friendly manufacture of stretchy TENGs for self-powered nano-systems in bio-medical and conservational applications (Yang et al., 2014b).

Cross-linked blend films such as ChS and PVA that contain both ionic and covalently bound ions and mobile counter ions transfer some of their mobile electrons to transport charges to another material upon contact. According to the charge transfer model, contact separation electrification yields ChS and PVA as a net electrostatic charge source (Chen et al., 2013; Mallineni et al., 2017). The proposed novel ChS-PVA has advantages such as a special electronic charge through nanochannels that comprise $–NH_2$ and OH functional groups for ion transfer and interconnected fused aliphatic chain bridges for electron transfer. This empowers the ChS-PVA TENG to permit long-lasting electrostatic, depending on the interaction surface, which can create disproportion among the number of electric charges on the membrane surface that can alter the triboelectric-exposed circuit voltage (Voc) and short circuit currents (Jsc). The induced charges of the ChS-PVA film are comparative to the external area of the membrane and are near to the hypothetical limit, made compulsory by the dielectric breakdown of air (Chen et al., 2013; Yang et al., 2013; Tang et al., 2014; Yang et al., 2014a; Yang et al., 2014c; Shin et al., 2016). However, a noteworthy claim is revealed to improve the triboelectric polarization by altering their morphologies, chemical construction, and interpenetration of ionic functional assemblies through cross-linking within the polymer network. The proposed novel polymeric ChS-PVA TENG is able to demonstrate strong chemical stability, tensile modulus, and strength to improve the triboelectric current (Chen et al., 2013; Fan et al., 2015). The flexible Chs-PVA membrane

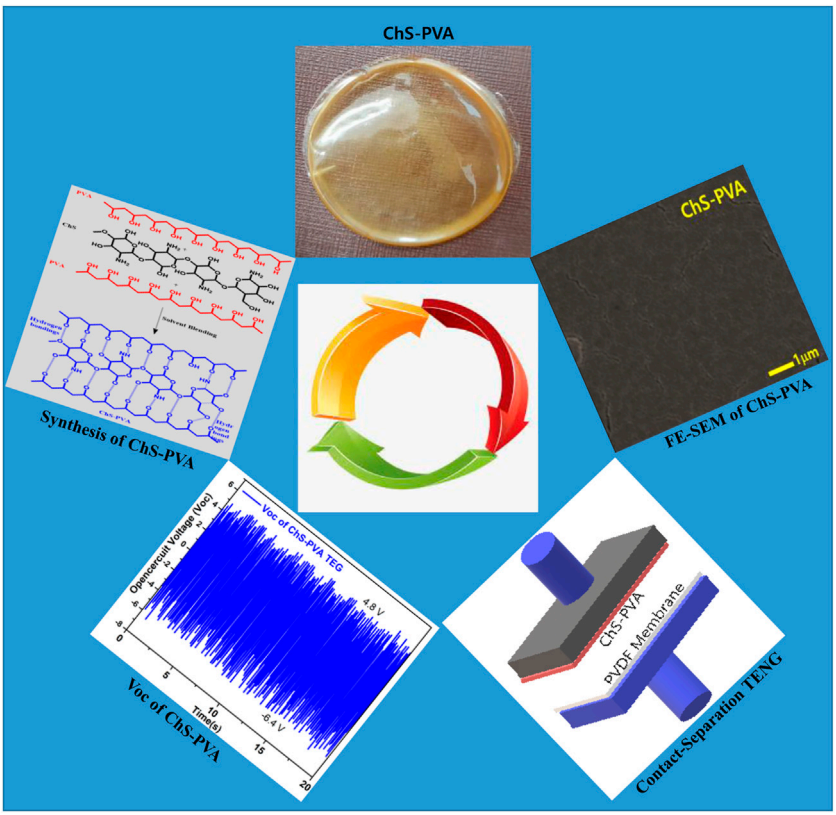

FIGURE 1 | Schematic illustration for the synthesis of ChS-PVA biopolymer membrane and contact-separation TENG.

surged the output voltage (Voc) of 21.2 V, and short circuit current (Isc) of 514 nA at 5 Hz, respectively. The Voc and Isc enhancements of the ChS-PVA TENG were observed when compared with the ChS TENG, and the PVA TENG with the enhancement of Voc and Isc of the ChS-PVA TENG were 244, and 1,080% from the ChS TENG. Where, as in the case of the PVA TENG, the enhancement of Voc and Isc were increased by 633 and 2,888%, respectively due to due to availability of a free loan pair on -NH_2 and -OH functional assemblies, as shown in **Figure 1**.

EXPERIMENTAL SECTION

Materials and Methods

Chitosan was purchased from the Aldrich Chemical Co., United States. The grade of deacetylation is about 80%, and molecular weight is about 400,000 Da. Acetic acid and PVA were obtained from Aldrich Co. Ltd., and used as received.

Preparation of the Chitosan, Polyvinyl Alcohol, and Chitosan-Polyvinyl Alcohol Films

A total of 1.0 g of ChS was taken in 80 ml of 2 %V/V of acetic acid solution (2 ml acetic acid/100 ml of water). The clear solution was obtained in 1 h, and degassed and cast on the Petri-dish to generate the ChS membrane. A total of 5 wt% of PVA was mixed and was cast on the glass plate to obtain the transparent PVA membrane. A total of 1.0 g of ChS was dissolved in 80 ml of 2 %V/V of acetic acid solution. After stirring for 1 h, 5 g of PVA was taken in 95 ml of DI water, and stirred at 90 °C for 5 h. A total of 1 g of 5 wt% PVA solution was mixed with 1 g of 1 wt% ChS solution and stirred for 12 h to obtain the homogenous polymeric mixture. The 10 g of blended ChS-PVA polymeric mixture was degassed, and cast onto the glass plate to obtain the transparent membrane with a thickness of 50 microns. The film thickness is a very significant restriction in determining the films' physical properties. The films had an average width of 50±2 μm and visually, the films were moderately transparent with a pale yellow color (**Figure 2**).

FTIR, SEM, and X-ray Diffraction Spectroscopy Electrical Output Characterizations

The FT-IR spectra of the ChS, PVA, and ChS-PVA biopolymer films were scanned using an IFS66V/S and HYPERION 3000, Bruker Optiks (Germany). X-ray diffraction (XRD) of ChS, PVA, and ChS-PVA biopolymers was measured by a DMAX-Ultima III X-ray diffractometer between 5° and 50° theta. SEM observations

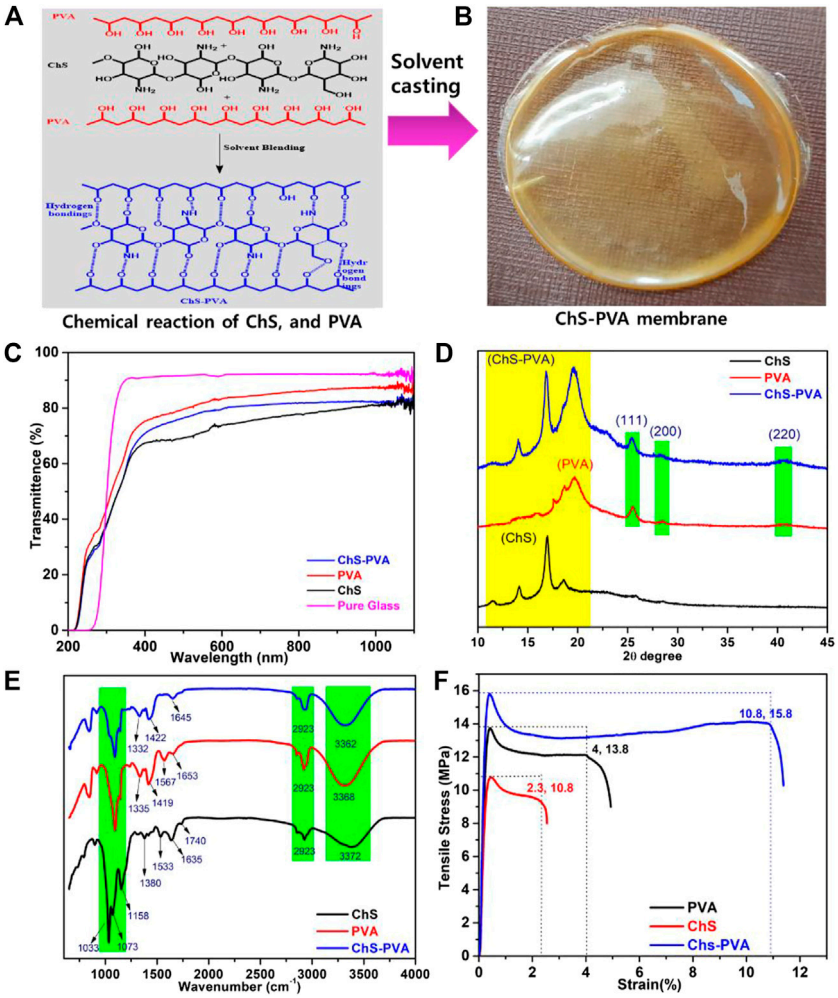

FIGURE 2 | (A) Chemical structure, **(B)** digital image, **(C)** UV-Vis transmittance spectra, **(D)** XRD patterns, **(E)** FT-IR, and **(F)** stress-strain curves of the ChS, PVA, and ChS-PVA biopolymer films.

were carried out on an FEI Sirion FE-SEM, 30 kV microscope. The films were thoroughly dried before capturing the images, and the surface morphology images were studied.

The production signals of the ChS TENG, PVA TENG, and ChS-PVA TENG were periodically constrained and released by an oscillator, and subsequent electrical signals were measured by a Keithley Digital Multi Meter (KDMM). Later, the impact force was determined via load cell YC33-5K (SETECH) at various applied frequencies of 1, 2, 3, 4, and 5 Hz, correspondingly.

Tensile-Stress Curves

The tensile strength, modulus properties, and elongation of the ChS, PVA, and ChS-PVA tissues were determined using a table-top common testing machine (AGS-X+250, Shimadzu Corp., Japan) furnished with a 1 kN load cell. The test speediness was fixed at a rate of 10 mm/min. The gauge length between the grips was 10 mm. All tested examples were a regular quadrilateral shape after being dried at room temperature.

Fabrication of the Chitosan-Polyvinyl Alcohol Triboelectric Nanogenerators Scheme

The construction and the operational source of the contact and separation mode of the ChS-PVA TENG are discussed in this section. Here, the structure of the TENG model is depicted in **Figure 5**. First, the ChS-PVA membrane and TENG were developed by attaching the ChS-PVA membrane with the measurements of 3 cm × 3 cm = 9 cm^2 on an Al electrode. Then, the ChS-PVA TENG electrode was changed to commercial foam to reduce the imitating force while contact and separation continued. Secondly, the Al electrode remained located on the PVDF skin with similar sizes along with the supporting foam. Then, the two conductors were placed inside the mainspring structure (which was made of four identical flexible mainsprings with two distinct dielectric surfaces with a distance of 40 mm), and a load cell was coupled to the top of the Al electrode in order to quantity the load force while the

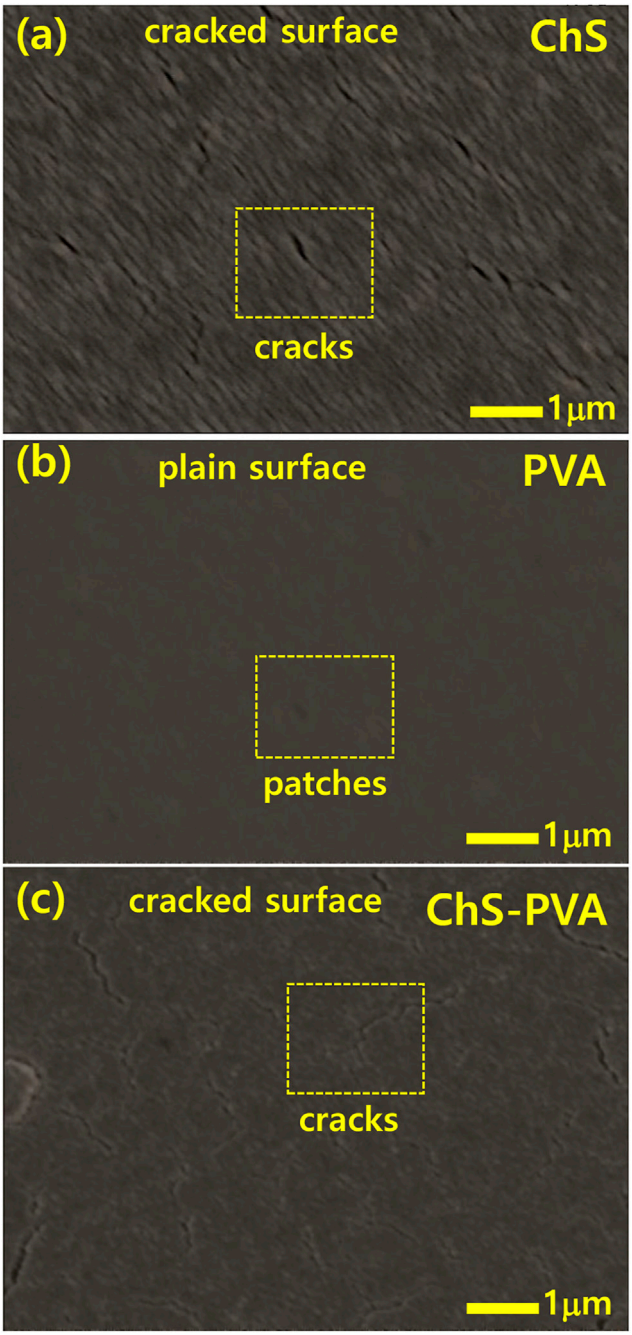

FIGURE 3 | Representative surface SEM images of **(A)** ChS, **(B)** PVA, and **(C)** ChS-PVA biopolymers films.

triboelectric surfaces made contact with each other. A similar protocol was followed for the other ChS TENG and PVA TENG. In the meantime, a rectilinear oscillator containing a DC motor powered with an eccentric system steadily wavered by a linear slider at 5 Hz. The cautious location of the overall system resulted in a switchable interaction between the ChS-PVA film and the PVDF film, whereas the slider oscillation was consistent.

RESULTS AND DISCUSSION

Appearance and Thickness of the Chitosan-Polyvinyl Alcohol Biopolymer Film

Figure 2 shows the ChS, PVA, and ChS-PVA biopolymer films and their physico-chemo-mechanical properties. The chemical structure of the ChS-PVA composite film was visually plain with no rigid zones, bubble-free, flexible, and could be easily skinned from the casting plates (**Figure 2A**). The ChS-PVA was miscible in all combinations used in this study, and this was recognized to construct the strong inter-molecular hydrogen bonds between the ChS and PVA polymers. Film thickness is a very significant restriction in determining a film's physical properties. The films had an average width of 50±2 μm and visually, the films had a moderately transparent pale yellow color (**Figure 2B**) (Cheedarala and Song, 2019a; Cheedarala and Song, 2019b).

Optical Properties (UV-Vis Transmittance Spectroscopy)

One of the important features of a wrapping flexible solid is that it should defend food from the effects of light, especially UV radiation. Recently, Dajian et al. studied a chitosan/PVA nanocomposite film reinforced with halloysite nanotubes where they reported that the optical properties and the samples were highly transparent with light transmittance using UV-vis spectra (Cheedarala et al., 2019). To determine the light transmission properties of the films, they were scanned at wavelengths extending from 200 to 800 nm, and the fraction light transmission was recorded. Similarly, our ChS-PVA also showed similar UV-vis results in transmittance mode. Generally, the membrane samples were exhibited at low light transmission in UV light, especially at wavelengths of 280 nm, as shown in **Figure 2C**.

X-ray Diffraction

X-ray diffraction (XRD) analysis of the ChS-PVA biopolymer membrane was confirmed with their pristine ChS and PVA films and can affect the crystallinity of the ChS-PVA, as shown in **Figure 2D**. We found two distinct diffraction peaks that appeared as a strong sharp peak and a broad peak at 2 θ values of 20°, 18° and 12° that provided clear evidence of the amorphous nature of ChS (Cheedarala et al., 2018a). On the other hand, the PVA showed broad to sharp peaks at 42° (220), 29° (200), 28° (111), 20° representing the amorphous nature of the PVA polymer. The peak shifts and shape were changed by the ChS-PVA biopolymer blend membrane matrix. The intensity of the characteristic ChS-PVA peaks were increased due to the increase of crystallinity by the cross-linking effect. Therefore, the chemical structure of the ChS and PVA biopolymer films changed dramatically with the increasing chemical crosslinking through hydrogen bonding, indicating that there were strong chemical interactions between the ChS and PVA.

FT-IR

The FT-IR spectrum of the ChS, PVA, and ChS-PVA films were in good agreement with reported literature (Huang et al., 2012; Jeon et al., 2013; Cheedarala et al., 2018; Nahian et al., 2017). In particular, the characteristic peaks of ChS, viz., the -OH, -CH, -CO amide I, and amide II functional groups appeared at

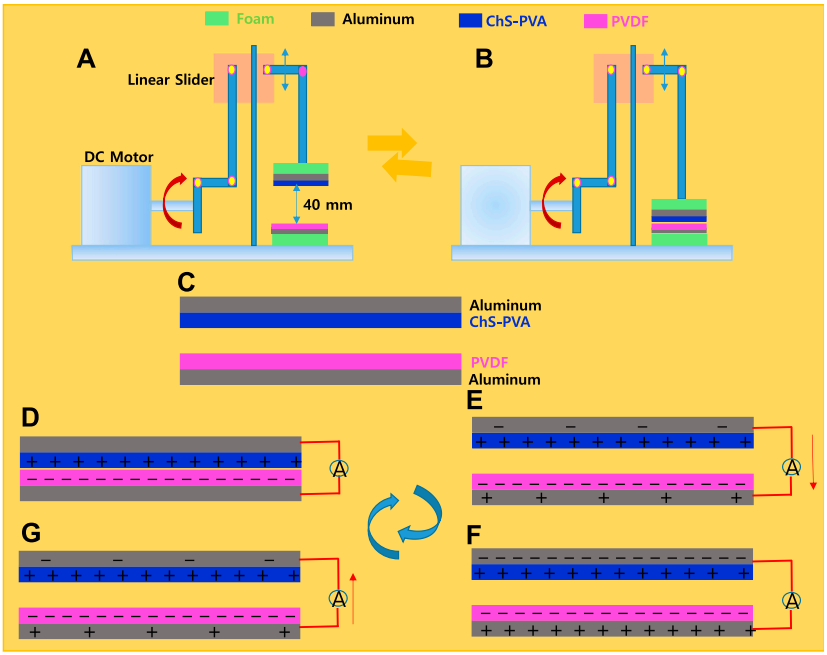

FIGURE 4 | Mechanical manipulation of the ChS-PVA TENG at **(A)** the separation state, **(B)** the contact state, and working mechanism at **(C)** the initial condition, **(D)** full contact, **(E)** separating, **(F)** full separation, and **(G)** contact again.

3372 cm^{-1}, 2923 cm^{-1}, 1740 cm^{-1}, 1635 cm^{-1}, and 1533 cm^{-1}, respectively. Also, the peaks at 1380 cm^{-1}, 1158 cm^{-1}, and 1073 cm^{-1}, 1033 cm^{-1}, and 617 cm^{-1}, were the strong stretching vibration of the -CH_2OH of C_6 position of the sugar moiety CH_2 (ben), CH (deform), CO (str), and other related peaks, respectively (Cheedarala et al., 2015). The FT-IR of PVA showed significant absorption bands at 3368 cm^{-1}, 2923 cm^{-1}, 1663 cm^{-1}, 1419 cm^{-1}, 1335 cm^{-1}, and 1080 cm^{-1} for -OH, -CH_2, -CO, CH_2 (ben), CH (deform), and CO (str), respectively. The FT-IR spectrum of the ChS-PVA blend membrane showed significant changes from the pure ChS and PVA due to crosslinking of both the polymers. The ChS-PVA membrane revealed the differences between their respective absorbance bands at 1645 cm^{-1}, 1422 cm^{-1}, 1332 cm^{-1}, and 1031 cm^{-1}, indicating the crosslinking effect between ChS and PVA. Thus, the results of FT-IR analysis clearly proved the formation of the homogeneous dispersion of the polyelectrolyte complex through interfacial adhesion between ChS-PVA blend films, as shown in **Figure 2E**.

Tensile Test

Due to the crosslinking of the ChS-PVA blended polymer matrix, the strong interactions between the ChS and PVA films had strong reinforcement. To demonstrate this reinforcement, tensile tests were achieved for all ChS, PVA, and ChS-PVA blend films. The typical stress-strain curves are shown in **Figure 2F**. The results indicated that the strain (%) and tensile modulus (MPa) of ChS and PVA were 2.3 and 10.8, and 4 and 13.8, respectively. The ChS-PVA membrane showed a higher strain (%) and tensile modulus (MPa) of 10.8 and 15.8 due to chemical crosslinking through the strong hydrogen bonding between ChS and PVA. The tensile strength (MPa) and strain (%) of the ChS-PVA membrane showed 369 and 46% over pristine ChS, and 170 and 14.5% over pure PVA films, respectively due to the ChS-PVA membrane blending though chemical interactions (Jeon et al., 2013).

FE-SEM Interpretation

To study the surface morphologies of ChS, PVA, and ChS-PVA blend films, FE-SEM analysis was employed, as shown in **Figure 3**. The regular cracks and pores were found on the ChS surface due to the formation of oxidative air gaps (**Figure 3A**). The PVA membrane matrix showed a densely packed surface with irregular patches (**Figure 3B**). The ChS-PVA blend membrane showed regular homogeneity confirming the strong chemical interactions that include ionic cross-linking and the strong hydrogen bonding of the blend membrane of ChS-PVA (**Figure 3C**). However, the magnified surface image had continuous cracks and pores. To clearly understand the surface morphology of the polyelectrolytic ChS-PVA (pore size, symmetry, and network structure), the samples were generated by atmospheric oxidation on the surface. However, to generate the high output voltage and currents, the surface morphology played a pivotal role (Cheedarala et al., 2011; Cheedarala et al., 2014; Cheedarala et al., 2018; Cheedarala and Song, 2019; Cheedarala, 2021).

Set-Up of Chitosan-Polyvinyl Alcohol Triboelectric Nanogenerators

Figures 4A,B show the mechanical set-up of the ChS-PVA TENG in its full separation and contact state,

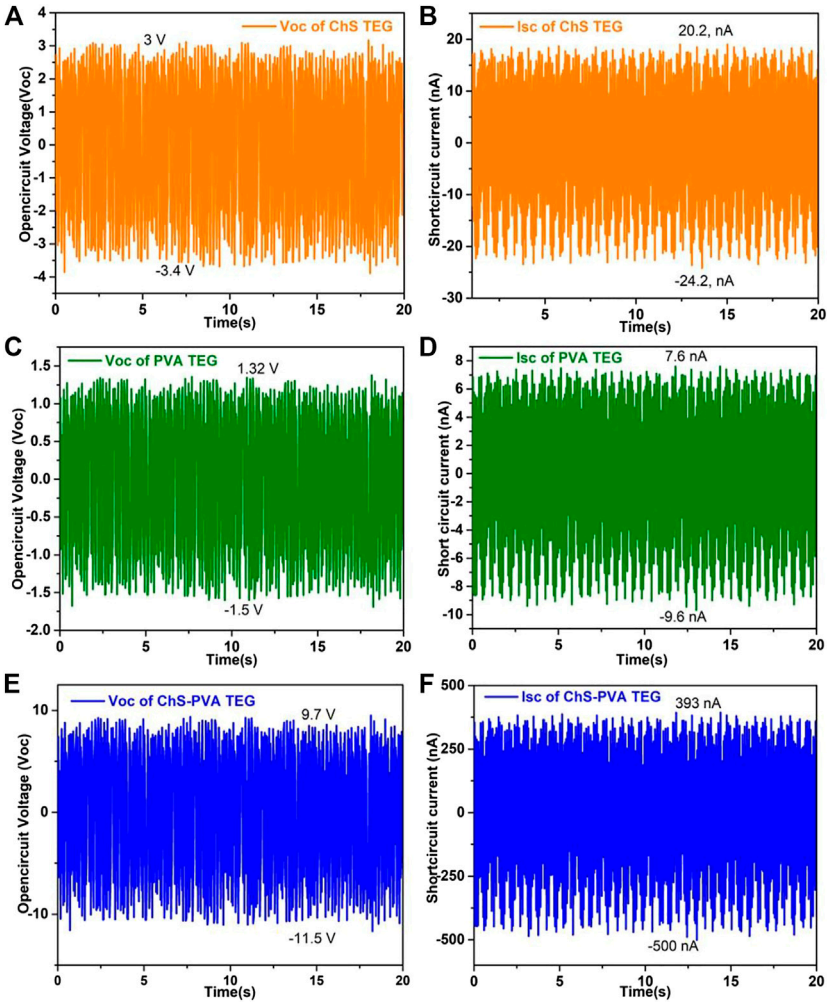

FIGURE 5 | Overall output voltages (Voc) and short circuit currents (Isc) of **(A, B)** ChS TENGs; **(C, D)** PVA TENGs; and **(E, F)** ChS-PVA TENGs at 5 Hz.

correspondingly, for effectively generating triboelectric power. The energy harvesting principle rigorously follows the contact electrification approach by the contact and separation of ChS-PVA and PVDF under the working mechanism of the developed ChS-PVA TENG elucidated here, whereby the polymeric surface and the Al conductors remained originally free of charge, as shown in **Figure 4C**. Conversely, after the fluctuation by the DC motor, the triboelectrically negative PVDF surface barely touched the surface of the ChS-PVA. The frequency variation of the PVDF surface thus became negatively charged and the ChS-PVA surface became completely positive charged due to the contact electrification, as shown in **Figure 4D**. During the interaction electrification process, these charges were endured for a lengthier period of time due to the shielding properties of the material (Fan et al., 2015). Because of the superior hydrophobic properties of the PVDF membrane (contact angle, CA~116°), it maintained the dry nature on the surface and an effective charge separation happened when it was separated from the ChS-PVA surface. In this circumstance, the two Al electrodes were strongly induced to attain charges by the ChS-PVA and PVDF in order to continue without bias so that the top conductor was negatively charged, and the bottom electrode was positively charged. During this departure procedure, the charges were fed through an external load, and the current flow happened, as shown in **Figure 4E**. The current was stationary as the two surfaces were completely detached, and a new equilibrium state was reached (**Figure 4F**). When the ChS-PVA and PVDF layers were in a closing state, the electrostatic induction became increasingly stronger such that it bankrupted the equilibrium, and resulted in charge redistribution of Al electrodes through the receiving and release of electrons, as shown in **Figure 4G**. It was significant that the current flow was in the opposite track. As soon as the two layers were completely closed, the charge-transfer procedure vanished and there was no current at all (Cheedarala and Song, 2019; Cheedarala and Song, 2019).

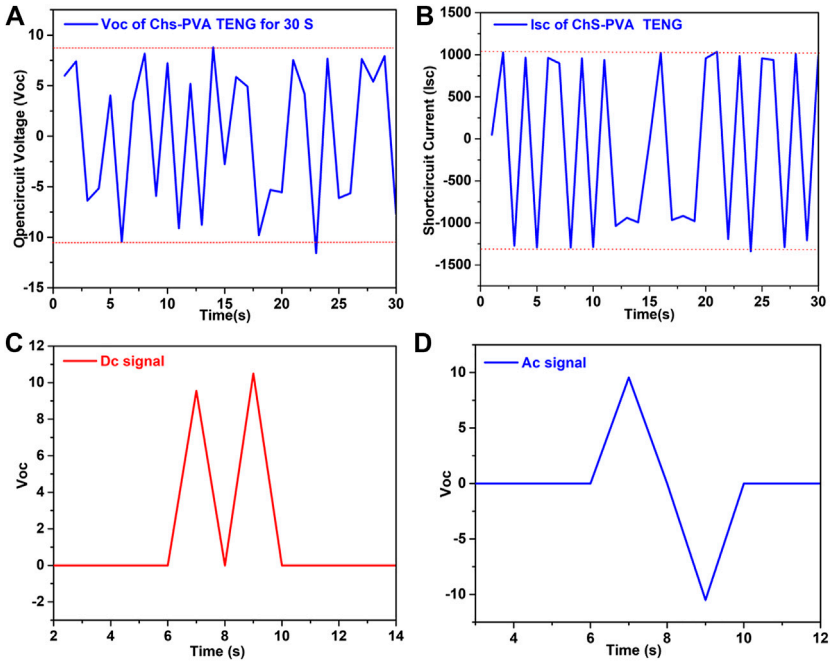

FIGURE 6 | Performance characteristics of the ChS-PVA TENG with sign wave signals of Voc. **(A)** Isc, **(B)** rectified voltage, **(C)** DC signal, and **(D)** AC signal at 5 Hz.

Results of Chitosan-Polyvinyl Alcohol Triboelectric Nanogenerators Against to PVDF Membrane

To validate the principle, we first measured the power output of the ChS TENG through the contact separation mode at 5 Hz. **Figure 5A** shows that the open-circuit Voc of the ChS TENG at 5 Hz surged from −3.4 to 3 V (6.4 V) upon detachment. Also, the charge transported among the Al conductors promptly produced short-circuit current Isc. The peak value of the Isc reached from −24.2 to 20.2 nA (44.4 nA) as shown in **Figure 5B**. Next, the Voc and Jsc of the PVA TENG showed a surge from −1.5 to 1.32 V (2.82 V) and from −9.6 to 7.6 nA (17.2 nA) at 5 Hz, respectively, as shown in **Figure 5C** and 5 days. On the other hand, the flexible ChS-PVA membrane surged the output voltage from -11.5 to 9.7 V (21.2 V), and short circuit current from -393 nA to -500 nA (893 nA), respectively, as shown in **Figures 5E,F**. The Voc and Isc enhancements of the ChS-PVA TENG were observed when compared with the ChS TENG and PVA TENG, respectively (Cheedarala et al., 2018; Cheedarala et al., 2019). The enhancement of Voc and Isc of the ChS-PVA TENG were 244% and 1,911% over the ChS TENG. Where, as in the case of the PVA TENG, the enhancement of Voc and Isc increased by 633% and 5,091%, respectively due to the availability of a free loan pair on the -NH_2 and -OH functional groups. The loan-paired electrons were ready to expel the plentiful static charges when the negatively charged PVDF membrane was contacted. After chemical blending of ChS and PVA, the ChS-PVA flexible membrane showed greatly improved Voc and Isc (Cheedarala et al., 2018).

We measured the electrical output of the ChS-PVA TENG and found sign wave signals from 0 to 1 m at 5 Hz applied frequency. The sign wave signals were observed in both output voltage and currents, it indicated that the output signals were in a sinusoidal wave motion, as shown in **Figures 6A,B** (Huang et al.). The rectified outputs of the prepared ChS-PVA TENG with a unidirectional output could be deposited in energy loading devices such as capacitors and batteries. The performance stability of the proposed ChS-PVA TENG was tested at 5 Hz applied frequency. The DC signal showed that a unidirectional and AC signal appeared bidirectionally, as shown in **Figures 6C,D**, respectively due to storage devices such as capacitors and batteries (Huang et al.). Also, the extraordinary energy gathering properties and greater mechanical assets were shown by the ChS-PVA TENG. The Voc of ChS and PVA were very low compared to the ChS-PVA TENG due to the absence of plentiful electronic transfer functional groups on their surfaces. Therefore, we modified the ChS and PVA into a combined ChS and PVA to enhance its triboelectric potential (Cheedarala et al., 2018b).

Next, we attempted to determine the impact force at various frequencies. The load cell YC33-5K (SETECH) was used to quantify the contact force and the result is shown. Meanwhile, a rectilinear oscillator containing a DC motor with a crank system was steadily vacillating by a linear slider. The cautious setting of the complete system caused a switchable contact between the ChS-PVA surface and the PVDF surface when the slider oscillation was reliable, as shown in **Figures 7A,B**. Built on the investigative results, the change of impact force increasingly upsurged with respect to the contact frequencies of 1, 2, 3, 4, and 5 Hz, and established the increment of Voc and Isc (Cheedarala et al., 2016a; Kong et al., 2016). When more

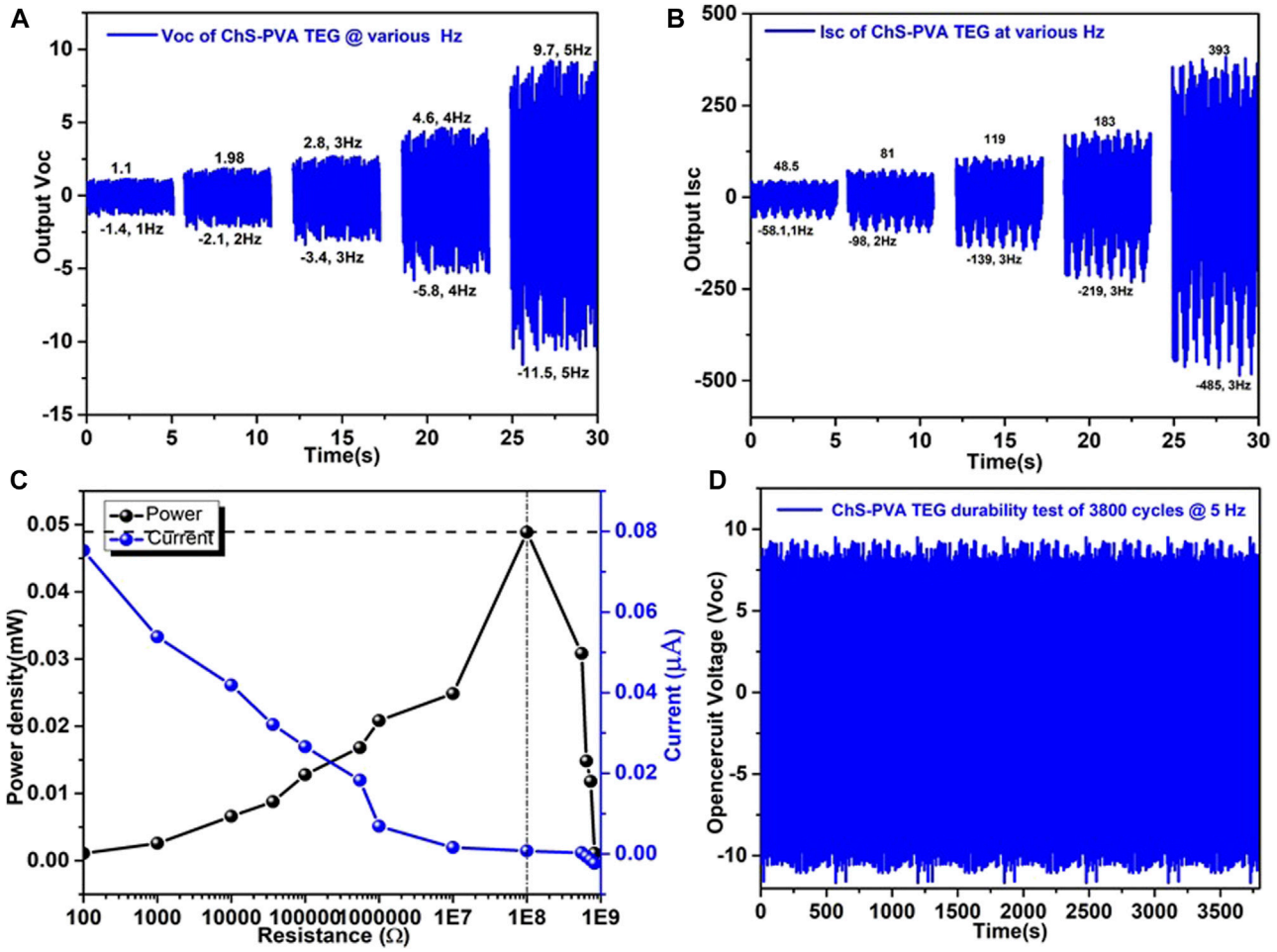

FIGURE 7 | The output performance of the ChS-PVA TENG at various speeds of various frequencies using a contact separation mode mechanical device **(A)** Voc; **(B)** Isc; and **(C)** the comparison of Isc (μA) and power density (mW) under different applied frequencies of the ChS-PVA TENG.

impact force was applied, the more real area was covered, which meant a higher output current was produced. The Voc and Isc were generated for 2.5 V (1 Hz), 4.08 V (2 Hz), 6.2 V (3 Hz), 10.4 V (4 Hz), and 20.8 V (5 Hz), and 107 nA (1 Hz), 179 nA (2 Hz), 258 nA (3 Hz), 660 nA (4 Hz), and 878 nA (5 Hz), respectively (Cheedarala et al., 2011; Cheedarala et al., 2014; Cheedarala et al., 2015). Also, we measured the electric output of the ChS-PVA TENG upon connecting directly to an external load of different resistors. The peak instantaneous Isc of the ChS-PVA TENG was measured at 5 Hz oscillation. It was noted that the peak Isc decreased with an increment of the resistance. Consequently, the maximum instantaneous power output of the ChS-PVA TENG was 0.48 mW at 100 MΩ and decreased continuously with the increment of resistance, due to low current by default of ohmic loss, as shown in **Figure 7C**. The performance stability of the proposed ChS-PVA TENG was tested for ~3800 cycles, as shown in **Figure 7D**. Open circuit voltage has been measured at 5 Hz contact frequency, and almost persistent Voc except some fluctuations where the Voc has been observed throughout the whole period of the stability and durability test. This is due to the exceptional energy harvesting properties and superior mechanical strength of the ChS-PVA TENG surface (Cheedarala and Song, 2019c; Cheedarala and Song, 2019d; Cheedarala, 2021; Cheedarala and Song, 2021).

CONCLUSION

In this article, we fabricated a simple and highly resilient ChS-PVA membrane by a simple solution casting method to generate a highly transparent membrane with tunable mechanical properties. This method is lucrative and modest for the production of high V_{oc} and I_{sc}. The modification of ChS and PVA was obtained through a series of experiments such as solution mixing of both ChS and PVA solutions and generating the high quality membrane through the drop casting method. Superior mechanical properties were observed from the ChS-PVA membrane compared to their pristine films. The FT-IR and XRD analyses discovered the functional group

determinations on the modified ChS-PVA surface that facilitated us to appraise the connections both chemically and electrically between the ChS-PVA and PVDF. The electronegativity of PVDF was very much encouraged to outshine higher currents at ambient circumstances. The V_{oc}, and I_{sc} of the ChS TENG, PVA TENG, and ChS-PVA TENG were 6.4 V and 44.4 nA, 2.82 V and 17.2 nA, and 22 V and 514 nA, respectively. The enhancement of V_{oc} and I_{sc} of ChS-PVA TENG were 244 and 1,080% from the ChS TENG. Where, in the case of the PVA TENG, the enhancement of V_{oc} and I_{sc} increased by 633 and 2,888%, respectively due to the availability of a free loan pair on the -NH_2 and -OH functional groups. Our projected ChS-PVA showed remarkably vigorous and consistent energy gathering presentations due to the mechanically strong material properties of the ChS-PVA membrane using a simple solution process and has great potential for self-powered TENG systems even under various strict surroundings and in discrete medical applications without harmful effects. We are exploring detailed experimental results and will publish soon elsewhere.

DATA AVAILABILITY STATEMENT

The original contributions presented in the study are included in the article/Supplementary Material, further inquiries can be directed to the corresponding authors.

AUTHOR CONTRIBUTIONS

First author contribution idea generation, experiments, execution, research data analysis, manuscript writing. Second author research facilities.

FUNDING

National Research Foundation of Korea (NRF) Nos. 2018R1A6A1A03024509 and 2019R1A2C1011113.

REFERENCES

Cheedarala, R. K., Kim, G.-H., Cho, S., Lee, J., Kim, J., Song, H.-K., et al. (2011). Ladder-type Heteroacenepolymers Bearing Carbazole and Thiophene Ring Units and Their Use in Field-Effect Transistors and Photovoltaic Cells. *J. Mater. Chem.* 21, 843–850. doi:10.1039/c0jm01897j

Cheedarala, R. K., Jeon, J.-H., Kee, C.-D., and Oh, I.-K. (2014). Bio-Inspired All-Organic Soft Actuator Based on a π-π Stacked 3D Ionic Network Membrane and Ultra-fast Solution Processing. *Adv. Funct. Mater.* 24, 6005–6015. doi:10.1002/adfm.201401136

Cheedarala, R. K., Park, E. J., Park, Y.-B., and Park, H. W. (2015). Highly Wettable CuO: graphene Oxide Core-Shell Porous Nanocomposites for Enhanced Critical Heat Flux. *Phys. Status Solidi A.* 212, 1756–1766. doi:10.1002/pssa.201431858

Cheedarala, R. K., Park, E., Kong, K., Park, Y.-B., and Park, H. W. (2016a). Experimental Study on Critical Heat Flux of Highly Efficient Soft Hydrophilic CuO-Chitosan Nanofluid Templates. *Int. J. Heat Mass Transfer* 100, 396–406. doi:10.1016/j.ijheatmasstransfer.2016.04.096

Cheedarala, R. K., Parvez, A. N., and Ahn, K. K. (2018a). Electric Impulse Spring-Assisted Contact Separation Mode Triboelectric Nanogenerator Fabricated from Polyaniline Emeraldine Salt and Woven Carbon Fibers. *Nano Energy* 53, 362–372. doi:10.1016/j.nanoen.2018.08.066

Cheedarala, R. K., Duy, L. C., and Ahn, K. K. (2018b). Double Characteristic BNO-SPI-TENGs for Robust Contact Electrification by Vertical Contact Separation Mode through Ion and Electron Charge Transfer. *Nano Energy* 44, 430–437. doi:10.1016/j.nanoen.2017.12.019

Cheedarala, R. K., Shahriar, M., Ahn, J. H., Hwang, J. Y., and Ahn, K. K. (2019). Harvesting Liquid Stream Energy from Unsteady Peristaltic Flow Induced Pulsatile Flow-TENG (PF-TENG) Using Slipping Polymeric Surface inside Elastomeric Tubing. *Nano Energy* 65, 104017. doi:10.1016/j.nanoen.2019.104017

Cheedarala, R. K., and Song, J. I. (2019a). Face-Centred Cubic CuO Nanocrystals for Enhanced Pool-Boiling Critical Heat Flux and Higher Thermal Conductivities. *Int. J. Heat Mass Transfer* 162, 120391

Cheedarala, R. K., and Song, J. I. (2019b). *In situ* generated Hydrophobic Micro Ripples via π-π Stacked Pop-Up Reduced Graphene Oxide Nanoflakes for Extended Critical Heat Flux and Thermal Conductivities. *RSC Adv.* 9 (54), 31735–31746. doi:10.1039/c9ra04563e

Cheedarala, R. K., and Song, J. I. (2019c). *J. Mech. Eng. Automation* 9, 225–229.

Cheedarala, R. K., and Song, J. I., (2019d). Ionic Polymer-Metal Composite Electro-Active Nano-Biopolymer Actuator, *IEEE Xplore*, doi:10.1109/ICMECT.2019.8932104

Cheedarala, R. K., and Song, J. I. (2021). Thermally Exfoliated π-π Stacked Blustered Graphene Oxide as an Efficient Flame Retardant Soft Nano-bundles for Vinyl Ester Resin Composites. *Mater. Adv.* 2 (2021), 497–510. doi:10.1039/d0ma00813c

Cheedarala, R. K., (2021). "What does data sovereignty imply: what does it Look like?," in *Novel Nanomaterials*. Intechopen. doi:10.5772/intechopen.95324

Chen, J., and Wang, Z. L. (2017). Reviving Vibration Energy Harvesting and Self-Powered Sensing by a Triboelectric Nanogenerator. *Joule* 1, 480–521. doi:10.1016/j.joule.2017.09.004

Chen, J., Zhu, G., Yang, W., Jing, Q., Bai, P., Yang, Y., et al. (2013). Harmonic-Resonator-Based Triboelectric Nanogenerator as a Sustainable Power Source and a Self-Powered Active Vibration Sensor. *Adv. Mater.* 25, 6094–6099. doi:10.1002/adma.201302397

Fan, F.-R., Lin, L., Zhu, G., Wu, W., Zhang, R., and Wang, Z. L. (2012). Transparent Triboelectric Nanogenerators and Self-Powered Pressure Sensors Based on Micropatterned Plastic Films. *Nano Lett.* 12, 3109–3114. doi:10.1021/nl300988z

Fan, X., Chen, J., Yang, J., Bai, P., Li, Z., and Wang, Z. L. (2015). Ultrathin, Rollable, Paper-Based Triboelectric Nanogenerator for Acoustic Energy Harvesting and Self-Powered Sound Recording. *ACS Nano* 9, 4236–4243. doi:10.1021/acsnano.5b00618

Feng, H., Zhao, C., Tan, P., Liu, R., Chen, X., and Li, Z. (2018). Nanogenerator for Biomedical Applications. *Adv. Healthc. Mater.* 7, 1701298. doi:10.1002/adhm.201701298

Huang, D., Wang, W., Kang, Y., and Wang, A. (2012). A chitosan/poly(vinyl alcohol) nanocomposite film reinforced with natural halloysite nanotubes. *Polym. Composites* 33, 1693–1699. doi:10.1002/pc.22302

Jeon, J. H., Cheedarala, R. K., Kee, C.-D., and Oh, I. K. (2013). Dry-Type Artificial Muscles Based on Pendent Sulfonated Chitosan and Functionalized Graphene Oxide for Greatly Enhanced Ionic Interactions and Mechanical Stiffness. *Adv. Funct. Mater.* 23, 6007–6018. doi:10.1002/adfm.201203550

Jiang, X.-Z., Sun, Y.-J., Fan, Z., and Zhang, T.-Y. (2016). Integrated Flexible, Waterproof, Transparent, and Self-Powered Tactile Sensing Panel. *ACS Nano* 10, 7696–7704. doi:10.1021/acsnano.6b03042

Jiao, Y., Zheng, Y., Jaroniec, M., and Qiao, S. Z. (2015). Design of Electrocatalysts for Oxygen- and Hydrogen-Involving Energy Conversion Reactions. *Chem. Soc. Rev.* 44, 2060–2086. doi:10.1039/c4cs00470a

Karan, S. K., Maiti, S., Lee, J. H., Mishra, Y. K., Khatua, B. B., and Kim, J. K. (2020). Recent Advances in Self-Powered Tribo-/Piezoelectric Energy Harvesters: All-In-One Package for Future Smart Technologies. *Adv. Funct. Mater.* 30, 2004446. doi:10.1002/adfm.202004446

Kong, K., Cheedarala, R. K., Kim, M. S., Roh, H. D., Park, Y. B., and Park, H. W. (2016). Electrical Thermal Heating and Piezoresistive Characteristics of Hybrid CuO-Woven Carbon Fiber/Vinyl Ester Composite Laminates. *Composites A: Appl. Sci. Manufacturing.* 85, 103–112.

Lin, Z., Chen, J., and Yang, J. (2016). *J. Nanomater.* 2016, 5651613

Maiti, S., Karan, S. K., Kim, J. K., and Khatua, B. B. (2019). Nature Driven Bio-Piezoelectric/Triboelectric Nanogenerator as Next-Generation Green Energy Harvester for Smart and Pollution Free Society. *Adv. Energ. Mater.* 9, 1803027. doi:10.1002/aenm.201803027

Mallineni, S. K., Dong, Y., Behlow, H., Rao, A. M., and Podila, R. (2017). *Adv. Energ. Mater.* 1702736, 1–

Moon, H., Chung, J., Kim, B., Yong, H., Kim, T., Lee, S., et al. (2017). Stack/flutter-driven Self-Retracting Triboelectric Nanogenerator for Portable Electronics. *Nano Energy* 31, 525–532. doi:10.1016/j.nanoen.2016.11.046

Nahian, S. A., Cheedarala, R. K., and Ahn, K. K. (2017). A Study of Sustainable Green Current Generated by the Fluid-Based Triboelectric Nanogenerator (FluTENG) with a Comparison of Contact and Sliding Mode. *Nano Energy* 38, 447–456. doi:10.1016/j.nanoen.2017.06.012

Shin, S. Y., Saravanakumar, B., Ramadoss, A., and Kim, S. J. (2016). Fabrication of PDMS-Based Triboelectric Nanogenerator for Self-Sustained Power Source Application. *Int. J. Energ. Res.* 40, 288–297. doi:10.1002/er.3376

Tang, W., Zhou, T., Zhang, C., Ru Fan, F., Bao Han, C., and Lin Wang, Z. (2014). A Power-Transformed-And-Managed Triboelectric Nanogenerator and its Applications in a Self-Powered Wireless Sensing Node. *Nanotechnology* 25, 225402–225408. doi:10.1088/0957-4484/25/22/225402

Wang, Z. L. (2013). Triboelectric Nanogenerators as New Energy Technology for Self-Powered Systems and as Active Mechanical and Chemical Sensors. *ACS Nano* 7, 9533–9557. doi:10.1021/nn404614z

Wang, Z. L., Chen, J., and Lin, L. (2015). Progress in Triboelectric Nanogenerators as a New Energy Technology and Self-Powered Sensors. *Energy Environ. Sci.* 8, 2250–2282. doi:10.1039/c5ee01532d

Wang, M., Li, W., You, C., Wang, Q., Zeng, X., and Chen, M. (2017). Triboelectric Nanogenerator Based on 317L Stainless Steel and Ethyl Cellulose for Biomedical Applications. *RSC Adv.* 7, 6772–6779. doi:10.1039/c6ra28252k

Wang, R., Gao, S., Yang, Z., Li, Y., Chen, W., Wu, B., et al. (2018). Engineered and Laser-Processed Chitosan Biopolymers for Sustainable and Biodegradable Triboelectric Power Generation. *Adv. Mater.* 30, 1706267. doi:10.1002/adma.201706267

Xie, Y., Wang, S., Niu, S., Lin, L., Jing, Q., Yang, J., et al. (2014). Grating-Structured Freestanding Triboelectric-Layer Nanogenerator for Harvesting Mechanical Energy at 85% Total Conversion Efficiency. *Adv. Mater.* 26, 6599–6607. doi:10.1002/adma.201402428

Yang, W., Chen, J., Zhu, G., Yang, J., Bai, P., Su, Y., et al. (2013). Harvesting Energy from the Natural Vibration of Human Walking. *ACS Nano* 7, 11317–11324. doi:10.1021/nn405175z

Yang, J., Chen, J., Liu, Y., Yang, W., Su, Y., and Wang, Z. L. (2014a). Triboelectrification-Based Organic Film Nanogenerator for Acoustic Energy Harvesting and Self-Powered Active Acoustic Sensing. *ACS Nano* 8, 2649–2657. doi:10.1021/nn4063616

Yang, J., Chen, J., Yang, Y., Zhang, H., Yang, W., Bai, P., et al. (2014b). Broadband Vibrational Energy Harvesting Based on a Triboelectric Nanogenerator. *Adv. Energ. Mater.* 4, 1301322. doi:10.1002/aenm.201301322

Yang, W., Chen, J., Jing, Q., Yang, J., Wen, X., Su, Y., et al. (2014c). 3D Stack Integrated Triboelectric Nanogenerator for Harvesting Vibration Energy. *Adv. Funct. Mater.* 24, 4090–4096. doi:10.1002/adfm.201304211

Zhang, X.-S., Han, M.-D., Wang, R.-X., Zhu, F.-Y., Li, Z.-H., Wang, W., et al. (2013). Frequency-Multiplication High-Output Triboelectric Nanogenerator for Sustainably Powering Biomedical Microsystems. *Nano Lett.* 13, 1168–1172. doi:10.1021/nl3045684

Zhang, B., Chen, J., Jin, L., Deng, W., Zhang, L., Zhang, H., et al. (2016). Rotating-Disk-Based Hybridized Electromagnetic-Triboelectric Nanogenerator for Sustainably Powering Wireless Traffic Volume Sensors. *ACS Nano* 10, 6241–6247. doi:10.1021/acsnano.6b02384

Zhang, N., Tao, C., Fan, X., and Chen, J. (2017). Progress in Triboelectric Nanogenerators as Self-Powered Smart Sensors. *J. Mater. Res.* 32, 1628–1646. doi:10.1557/jmr.2017.162

Zhu, G., Peng, B., Chen, J., Jing, Q., and Wang, Z. L. (2015). *Nano Energy* 14 (126), 2211–2855. doi:10.1016/j.nanoen.2014.11.050 CrossRef Full Text

Conflict of Interest: The authors declare that the research was conducted in the absence of any commercial or financial relationships that could be construed as a potential conflict of interest.

Copyright © 2021 Cheedarala and Song. This is an open-access article distributed under the terms of the Creative Commons Attribution License (CC BY). The use, distribution or reproduction in other forums is permitted, provided the original author(s) and the copyright owner(s) are credited and that the original publication in this journal is cited, in accordance with accepted academic practice. No use, distribution or reproduction is permitted which does not comply with these terms.